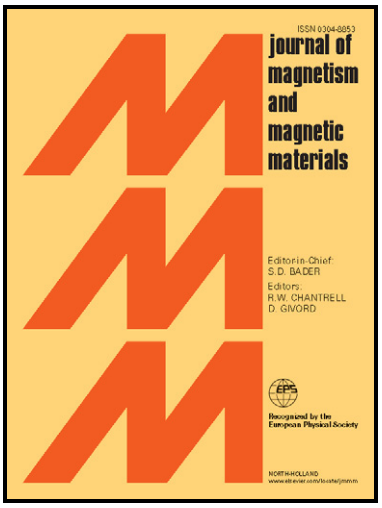

www.elsevier.com/locate/jmmm

Theoretical modelling of physiologically stretched vessel in magnetisable stent assisted magnetic drug targeting application

Adil Mardinoglu, P.J. Cregg, Kieran Murphy, Maurice Curtin, Adriele Prina-Mello

PII: S0304-8853(10)00671-2
DOI: doi:10.1016/j.jmmm.2010.09.028
Reference: MAGMA 56480

To appear in: *Journal of Magnetism and Magnetic Materials*

Received date: 27 July 2010
Revised date: 6 September 2010
Accepted date: 24 September 2010

Cite this article as: Adil Mardinoglu, P.J. Cregg, Kieran Murphy, Maurice Curtin and Adriele Prina-Mello, Theoretical modelling of physiologically stretched vessel in magnetisable stent assisted magnetic drug targeting application, *Journal of Magnetism and Magnetic Materials*, doi:10.1016/j.jmmm.2010.09.028

Theoretical Modelling of Physiologically Stretched Vessel in Magnetisable Stent Assisted Magnetic Drug Targeting Application

Adil Mardinoglu[a,*], P.J. Cregg[b], Kieran Murphy[b], Maurice Curtin[c], Adriele Prina-Mello[c,d,*]

[a] *Telecommunications Software & Systems Group (TSSG), Waterford Institute of Technology, Waterford, Ireland.*
[b] *Materials Characterisation and Processing Group, SEAM Centre, Waterford Institute of Technology, Waterford, Ireland*
[c] *Trinity Centre for Bioengineering, Trinity College, Dublin 2, Ireland.*
[d] *Centre for Research on Adaptive Nanostructures and Nanodevices (CRANN), Trinity College, Dublin 2, Ireland.*

Abstract

The magnetisable stent assisted magnetic targeted drug delivery system in a physiologically stretched vessel is considered theoretically. The changes in the mechanical behaviour of the vessel are analysed under the influence of mechanical forces generated by blood pressure. In this 2D mathematical model a ferromagnetic, coiled wire stent is implanted to aid collection of magnetic drug carrier particles in an elastic tube, which has similar mechanical properties to the blood vessel. A cyclic mechanical force is applied to the elastic tube to mimic the mechanical stress and strain of both the stent and vessel while in the body due to pulsatile blood circulation. The magnetic dipole-dipole and hydrodynamic interactions for multiple particles are included and agglomeration of particles is also modelled. The resulting collection efficiency of the mathematical model shows that the system performance can decrease by as much as 10 % due to the effects of the pulsatile blood circulation.

Key words: magnetic drug targeting, stretch vessel, magnetic nanoparticles, simulation, dipole-dipole interaction, hydrodynamic interaction, magnetizable

*Equal contribution to the paper and corresponding authors
Email addresses: mardinoglu@yahoo.com (Adil Mardinoglu), prinamea@tcd.ie (Adriele Prina-Mello)

stent.

PACS: 47.63.mh, 47.63.-b, 87.85.gf

1. Introduction

In the past ten years there has been a growing interest in the scientific and clinical application of magnetic drug carrier particles (MDCPs) as magnetic drug targeting (MDT) vehicles [1, 2, 3]. Although studies have shown that MDT is a relatively safe and effective methodology for targeting drugs to a specific site in the body [4], its implementation in clinical trials has been limited due to two fundamental issues. These issues which limit the applicability of the MDT approaches are the inherently weak magnetic force relative to the hydrodynamic forces, and the depth of the target zone from the surface of the skin. The most powerful permanent magnets can generate around 2 tesla homogeneous magnetic field and produce very small magnetic field gradients in the target zone. This makes MDCP collection problematic, because the magnetic force on a MDCP is proportional not only to the magnitude of the magnetic field but also to its gradient. Secondly, magnetic field strength, generated by a permanent magnet, decays with distance from the target zone and it is not enough to penetrate the biological tissue below 2 cm from the skin surface, to deliver MDCPs to reach their targeted site effectively. To overcome these limitations, ferromagnetic materials such as wires, seeds and stents are implanted into the body to increase the local magnetic field strength and this technique is called Implant Assisted Magnetic Drug Targeting (IA-MDT) [5, 6, 7, 8]. Typically IA-MDT models to date have assumed that vessel and implant are considered as rigid and not subjected to any mechanical forces. It is known that this is a limitation during the investigation of the biological response of IA-MDT systems since for clinical and biological relevance the vessel and the implanted stent are subjected to continuous mechanical forces due to pulsatile blood circulation [9]. Finite Element analyses have also been carried out to address the

stent-vessel deformation [10, 11, 12]. Changes in blood pressure or flow induce vessel remodelling and vessels are also under longitudinal stretch.

The main objective of this study is the modelling of a complex biological stent-vessel IA-MDT which encompasses of magnetic forces, fluid shear stresses and mechanical forces applied to stent and vessel. The response of vessels under physiological loading conditions is studied and a computationally based method that allows the analysis of the stress deformation evaluation in vessels is proposed. Residual stresses which have strong influence on the global radius response of the vessel and on the stress and strain distribution are also considered. The basic model geometry comprises a flexible, magnetisable coiled wire stent implant in close contact with the inner wall of a flexible biological vessel to mimic the mechanical constraint and strain of both stent and vessel as shown in Figure 1. Previously, some of the present authors developed and reported findings on a mathematical model which included both dipole-dipole and hydrodynamic interactions between multiple MDCPs and accounted for the agglomeration of the particles known to occur in the IA-MDT system [8], which allows closer agreement between theory and in vitro experiments. Here, results are presented for a stent-vessel undergoing cyclic stress deformation in order to examine the effect of stress deformations induced by pulsatile flow.

2. Outline of Model

In the human body, both vessel and implant are subjected to deformation ranging between 2.5% to 25% strain, ϵ. In this model, the flexible vessel is modelled as a circular cross section tubing with hyper-elastic material properties mimicking those of the cardiovascular tissue vessel [10]. The simulation is based on a simple sinusoidal waveform which is applied to the IA-MDT system for stretching the vessel with a frequency of 10 Hz and a strain rate of 10% which mimics a middle size vessel [13].

The model is based on 1 second strain activity which is divided into 40 equal time steps. Therefore previously developed model [8] parameters such as fluid

velocity, magnetic field strength and the resulting forces due to magnetic dipole-dipole interaction and hydrodynamic interaction will be changing at each time step due the changes in the geometry of flexible system.

In this model, we expand the model previously presented by Cregg *et al.* [8] where ferromagnetic particles with diameter of 0.86 μm containing 45.8 wt% magnetite are used as the MDCPs under the influence of homogeneous magnetic field oriented perpendicularly to the flow ($\theta = \pi/2$) with magnitudes of 0.15 T, 0.30 T, 0.45 T and 0.60 T. Stainless steel (SS) 430 is taken as the wire material for the flexible stent with a 62.5 μm radius. The stent is prepared by looping a length of wire into a 2 cm long coil, L, having a 0.04 cm radius containing 10 loops, N_l, with 0.2 cm between each loop (length of each loop), h. The coiled stent is positioned within a vessel in contact with the inner surface of the vessel (initial radius of 0.04 cm).

Nonlinear Finite Element Analysis (FEA) is commonly used to determine peak local strains on the stent subjected to physiological forces [14, 15]. Here, OpenFOAM [16] is used to calculate the strain applied to the stent-vessel during the modelling of pulsatile blood circulation. This allows the stent-vessel strain calculation to map the cyclic strain domain at the relevant conditions. This is important because of the nonlinear nature of mechanical behaviour, whereby the total strain is a combination of the material properties such as elasticity and plasticity [17].

The system performance is determined by considering the geometry and motion of each loop of the stent and this is proportional to the structural stiffness [18, 14, 15]. In case of coiled stent geometry, such performance depends on the basic geometrical parameters of the stent such as R_{wire}, R_{vessel}, N_l, length of a single loop, L_{loop}, and the angle of a loop, α, of the coiled stent. In this model, L_{loop} is recalculated in each time step to account for the physiological loading and it can be written as

$$L_{\text{loop}} = (2\pi R_{\text{vessel}}). \tag{1}$$

The axially applied load, F_{Z}, is the result of the fluid pressure which is

radially distributed along each single loop of the coil stent and it also depends on the α and L_{loop} ($F_{\text{Z}} = F_{\text{Z}}(\alpha, L_{\text{loop}})$). Since, the quantification of the strain, is related to the force applied to a single coil loop and it depends on the dynamic changes of the vessel-stent geometry at each sinusoidal cycle. This relationship can be shown as [18]

$$\epsilon = \left(F_{\text{Z}}/(\pi R_{\text{vessel}}^2)\right)/E \tag{2}$$

where, E is the Young modulus. This equation demonstrates that a number of geometric factors impact the stent strain.

In order to effectively model this system, the 3D geometry of the stent and vessel is reduced to 2D slice through the centre of the vessel (See Figure 1). Thus the coiled stent is modelled as a series of circular cross sections of an infinite wire with radius of R_{wire} located at the upper and lower boundaries of the walls. At each wall the wires are separated by a distance, h, between their centres, and the upper and lower sections are offset by $h/2$ as shown in Figure 1. It should be noted that physically this corresponds to a 2D description of flow with a parabolic profile in a rectangular box with transverse cylindrical wires, all of infinite extent. Under the physiological loading, the distance between the centres of the wires is recalculated at each time step to account for the changes in geometry of the stent and the cyclic mechanical deformation. In Figure 1, the CV has initial dimensions of 2 cm and 0.08 cm and encompasses a ten-loop stent within an expanded vessel. The MDCPs enter the CV from the left with the average inlet fluid velocity defined by a parabolic velocity profile.

For each time step, we model the behaviour of N ($N = 25$) MDCPs under the influence of i) Stokes drag, ii) hydrodynamic interaction forces, and iii) magnetic forces that account for the mutual magnetic dipole-dipole interactions. The effects of inertia and gravity are considered negligible and are ignored. For each time step, the Stokes drag for MDCP n, $\vec{F}_{\text{s}_n}$, is

$$\vec{F}_{\text{s}_n} = 6\pi\,\eta_{\text{f}}\,R_{\text{p}_n}\,(\vec{v}_{\text{f}} - \vec{v}_{\text{p}_n}), \tag{3}$$

where η_{f} is the viscosity of the fluid, R_{p_n} is the radius of MDCP n, and $\vec{v}_{\text{f}}$ and $\vec{v}_{\text{p}_n}$ are the velocities of the fluid and MDCP n respectively. The fluid

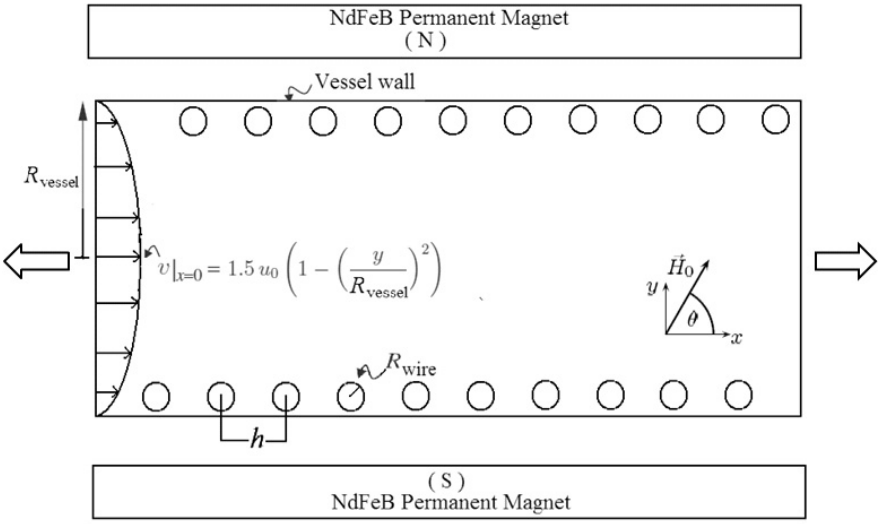

Figure 1: Schematic of the control volume (CV) used for determining the mechanically stretched magnetisable stent collection efficiency (CE) through analysis of the corresponding MDCP trajectories.

velocity, $\vec{v}_{\mathrm{f}}$, is determined by solving the appropriate Navier-Stokes equations. The motion of a MDCP through a viscous fluid creates a disturbance to the fluid flow, which is felt by all other MDCPs. As a result, the other MDCPs experience a force which is said to result from hydrodynamic interaction with the original MDCP. For each time step, by considering N MDCPs, the force due to the hydrodynamic interaction, $\vec{F}_{\mathrm{hyd}_n}$, which acts on MDCP n due to the presence of other $(N-1)$ MDCPs, can be written as

$$\vec{F}_{\mathrm{hyd}_n} = \sum_{\substack{i=1 \\ i \neq n}}^{N} \xi_{ni} \cdot \left(\vec{v}_{\mathrm{f}} - \vec{v}_{\mathrm{p}_i}\right) \tag{4}$$

where $\vec{v}_{\mathrm{p}_i}$ is the velocity of MDCP i and ξ_{ni} is the modification due to the hydrodynamic interaction given by

$$\xi_{ni} = -6\pi\,\eta_{\mathrm{f}}\,R_{\mathrm{p}_n}\,\frac{3\,R_{\mathrm{p}_i}}{4\,|\vec{r}_n - \vec{r}_i|}\left(\mathbf{1} + \frac{(\vec{r}_n - \vec{r}_i)\otimes(\vec{r}_n - \vec{r}_i)}{|\vec{r}_n - \vec{r}_i|^2}\right) \tag{5}$$

where R_{p_i} is the radius of the MDCP i, $\mathbf{1}$ is the unit tensor, $\otimes$ is the vector tensor product (outer product), $\vec{r}_n$ and $\vec{r}_i$ are the positions of MDCP n and MDCP i, respectively. Initially all MDCPs are taken to have the same radius but after agglomeration, MDCPs of different radius are possible, as each agglomeration is viewed as a new MDCP of increased radius.

Regarding the magnetic dipole-dipole interaction between N MDCPs, each MDCP is taken as spherical with radius R_{p_n} and sufficiently small to have homogeneous magnetic flux throughout the MDCPs. Hence, in each time step, in order to include the magnetic effect on MDCP n of the other $(N-1)$ MDCPs, the modified magnetic force, $\vec{F}_{\mathrm{mm}_n}$, can be written as

$$\vec{F}_{\mathrm{mm}_n} = (\vec{m}_n \cdot \nabla)\,\vec{B}_{\mathrm{total}_n} \tag{6}$$

where $\vec{m}_n$ is the total magnetic moment of MDCP n, $\vec{B}_{\mathrm{total}_n}$ is the total magnetic flux acting on MDCP n. It can be taken as

$$\vec{B}_{\mathrm{total}_n} = \vec{B} + \sum_{\substack{i=1 \\ i \neq n}}^{N} d\vec{B}_i \tag{7}$$

where $\vec{B}$ is the magnetic flux density due to the external field, $d\vec{B}_n$ is the modification of the resulting magnetic flux density due to MDCP n at $\vec{r}$. The modification to the magnetic flux density is thus taken as

$$d\vec{B}_n(\vec{r}) = \frac{1}{3}\left(\mu_0\, M_{\mathrm{fm,p,s}}\frac{L(\beta)}{B}\right)\ \frac{R_{\mathrm{p}_n}^3}{|\vec{r}-\vec{r}_n|^3}\left(\frac{3\left(\vec{B}(\vec{r}_n)\cdot(\vec{r}-\vec{r}_n)\right)}{|\vec{r}-\vec{r}_n|^2}(\vec{r}-\vec{r}_n)-\vec{B}(\vec{r}_n)\right) \tag{8}$$

where μ_0 is the magnetic permeability of free space, $L(\beta)$ is the Langevin function, B is the magnitude of the $\vec{B}$, $\vec{r}$ represents an arbitrary point in space, $\vec{B}(\vec{r}_n)$ is the flux density at $\vec{r}_n$ and $M_{\mathrm{fm,p,s}}$ is the saturation magnetisation of the ferromagnetic material in the MDCP. The value of $\vec{B}$ required to calculate the magnetic force as given by Eqs. (6) and (12), is calculated analytically from the scalar magnetic potential due to the stent wires as previously reported in Cregg *et al.* [8].

It is assumed that the ferromagnetic material in each MDCP consists of smaller single domain spherical nanoparticles. Thus, the average projection of $\vec{m}$ the moment in the direction of $\vec{B}_{\mathrm{total}}$ can be calculated from the Langevin function [19, 20, 6, 7, 8]

$$L\left(\beta\right) = \coth\left(\beta\right) - \frac{1}{\beta}, \tag{9}$$

with Langevin argument

$$\beta = \frac{m_{\mathrm{fm,p}}\, B_{\mathrm{total}}}{kT}, \tag{10}$$

where B_{total} is the magnitude of $\vec{B}_{\mathrm{total}}$, k is Boltzmann's constant, T is the absolute temperature and $m_{\mathrm{fm,p}}$ is the magnitude of the magnetic moment of the magnetite in the MDCPs. The magnetic moment of each magnetite nanoparticle within the MDCP, $\vec{m}_{\mathrm{fm,p}}$, can be written as

$$\vec{m}_{\mathrm{fm,p}} = V_{\mathrm{fm,p}}\, M_{\mathrm{fm,p,s}}\frac{\vec{B}}{B} \tag{11}$$

where $V_{\mathrm{fm,p}}$ is the spherical volume of a single domain magnetite nanoparticle and $M_{\mathrm{fm,p,s}}$ is the (volume) saturation magnetization of the magnetite inside the MDCPs.

Thus, the magnetic moment of the MDCP, $\vec{m}$, can be written as

$$\vec{m} = \omega_{\mathrm{fm,p}}\, V_{\mathrm{p}}\, M_{\mathrm{fm,p,s}}\, L\,(\beta)\, \frac{\vec{B}}{B} \tag{12}$$

where V_{p} is the MDCP volume and $\omega_{\mathrm{fm,p}}$ is the volume fraction of ferromagnetic material in the MDCP, related to its weight fraction [7, 8].

3. Fluid flow — the Navier-Stokes equations

The fluid is treated as an incompressible, Newtonian, isothermal, single-phase fluid with velocity $\vec{v}_{\mathrm{f}}$ and pressure P at steady state flow. We have the continuity equation

$$\nabla \cdot \vec{v}_{\mathrm{f}} = 0, \tag{13}$$

and the Navier-Stokes equation

$$\rho_{\mathrm{f}}[(\vec{v}_{\mathrm{f}} \cdot \nabla \vec{v}_{\mathrm{f}})] = \nabla P + \eta_{\mathrm{f}} \nabla^2 \vec{v}_{\mathrm{f}}, \tag{14}$$

where ρ_{f} is the density of the fluid. A parabolic velocity profile is assumed at the inlet control volume (CV) such that

$$v_{\mathrm{f},x|x=0} = 1.5\, u_0 \left(1 - \left(\frac{y}{R_{\mathrm{vessel}}}\right)^2\right), \tag{15}$$

$$v_{\mathrm{f},y|x=0} = 0 \tag{16}$$

where u_0 is the average inlet fluid velocity and R_{vessel} is the vessel radius. In this model, a constant flow rate is applied at the entrance of the CV and u_0 is recalculated in each time step to account for the change in diameter of the stretching vessel under mechanical forces. Furthermore, non-slip boundary conditions ($\vec{v}_{\mathrm{f}} = 0$) are applied at the wire-fluid interface and at the upper and lower CV boundaries. Atmospheric pressure is assumed at the outlet of the CV to satisfy the boundary condition on pressure.

4. Velocity equations, streamlines and system performance

The velocity of a MDCP n can be obtained by summing the Stokes drag, the force due to hydrodynamic interaction and the modified magnetic force, as given in Eqs. (3), (4) and (6) respectively with inertial forces, $\vec{F}_{\mathrm{i}_n}$, as

$$\vec{F}_{\mathrm{s}_n} + \vec{F}_{\mathrm{hyd}_n} + \vec{F}_{\mathrm{mm}_n} = \vec{F}_{\mathrm{i}_n}. \tag{17}$$

For MDCP n, by ignoring the inertial forces, $\vec{F}_{\mathrm{i}_n}$, we rewrite Eq. (17) as

$$6\pi\,\eta_{\mathrm{f}}\,R_{\mathrm{p}_n}\left(\vec{v}_{\mathrm{f}} - \vec{v}_{\mathrm{p}_n}\right) + \sum_{\substack{i=1 \\ i\neq n}}^{N} \xi_{ni}\cdot\left(\vec{v}_{\mathrm{f}} - \vec{v}_{\mathrm{p}_i}\right) + \left(\vec{m}_n\cdot\nabla\right)\left(\vec{B}_{\mathrm{total}}\right)_n = 0. \tag{18}$$

Hence, we can obtain $\vec{v}_{\mathrm{p}_n}$ by solving Eq. (18) numerically in each time step and the trajectories of each MDCP can be obtained from evaluating the streamline functions [6, 7, 8].

The system performance of this mathematical model is calculated in terms of collection efficiency, CE, defined as

$$\mathrm{CE} = \frac{2\,R_{\mathrm{vessel}} - y_1 + y_2}{2\,R_{\mathrm{vessel}}}\,100, \tag{19}$$

where y_1 and y_2 are defined by the location of the streamline at the entrance to the CV of the last MDCPs captured by the stent wires. All calculations were performed using the open-source software C++ finite volume library OpenFOAM [16] and the relevant fluid flow properties and the properties of the ferromagnetic material used in the MDCP and for the stent wire, are given in Table 1.

5. Results and Discussions

In this paper, we present the simulation results of the stretching of both stent and vessel under physiological loading conditions in an IA-MDT system. This model evaluates magnetic dipole-dipole and hydrodynamic interactions dynamically for each time step during the whole cyclic stretching of the system, which is divided in to 40 time steps. In the absence of mechanical forces generated by blood pressure which we term the rigid case, the fluid velocity and

Properties	**Symbol**	**Units**	**Values**
Applied Field Properties			
Magnitude	$\mu_0 H_0$	T	0.15, 0.30, 0.45, 0.60
Angle of field direction	θ	-	$\pi/2$
MDCP Properties			
Polymer material	-	-	P(S/V-COOH)Mag
Radius	R_p	μm	0.43
Density of the polymer material	$\rho_\mathrm{pol,p}$	kg/m^3	950
MDCP concentration	-	l^{-1}	4×10^{10}
Initial distance between the MDCPs	-	μm	29.24
MDCP Magnetic Material Properties			
Material	-	-	Magnetite
Weight content	$x_\mathrm{fm,p}$	wt%	45.8
Density of the magnetite material	$\rho_\mathrm{fm,p}$	kg/m^3	5050
Volume content	$\omega_\mathrm{fm,p}$	%	13.716
Saturation magnetisation	$M_\mathrm{fm,p,s}$	kA/m	350
Magnetic moment	$m_\mathrm{fm,p}$	Am^2	2.245×10^{-19}
Radius	$R_\mathrm{fm,p}$	nm	5.35
Stent Implant Properties			
Material	-	-	SS 430
Wire radius	R_wire	μm	62.5
Loop separation	h	cm	0.2
Number of loops	N_l	-	10
Coil length	L	cm	2
Saturation magnetisation	$M_\mathrm{implant,s}$	kA/m	1350
Magnetic susceptibility	$\chi_\mathrm{implant,0}$	-	1000
Fluid & Vessel Properties			
Injector Flow Rate		cm/s	$0.05, 0.10, 0.20, 0.40, 1.00, 2.00, 4.50$
Velocity	u_0	cm/s	$0.58 - 57.91$
Density	ρ_b	kg/m^3	1000
Viscosity	η_b	kg/ms	1.0×10^{-3}
Vessel radius	R_vessel	cm	0.04
Physical Properties			
Permeability of vacuum	μ_0	Tm/A	$4\pi \times 10^{-7}$
Temperature	T	K	300
Boltzmann's constant	k_B	J/K	1.38×10^{-23}

Table 1: Fluid and material parameters used in the stent based mathematical model.

the magnetic flux density are calculated once for the entire system. Here, under the physiological loading, the fluid velocity and the magnetic flux density are recalculated in each time step to account for the changes resulting from the mechanical stress.

The stent-vessel cross section and longitudinal length vary during the cyclic stretching whereas the volume of the entire stent-vessel system does not. Under the physiological loading, it should be noted that the injection velocity of the fluid is assumed constant and the inlet fluid velocity is recalculated through the change of the diameter of the vessel in each time step and the MDCP trajectories are plotted.

This new model is focused in a time step evolution of the initial position of N ($N = 25$) MDCPs at the entrance of the CV and presents the results in terms of the CE of the system considering the agglomeration of MDCPs. Since, this model requires the solution of multiple differential equations in each time step, the computational power required to account for 25 particles under the physiological loading is more than required in the rigid case.

We created a homogeneously distributed square cluster of $N = 25$ MDCPs at the entrance of the CV and placed the centre of the cloud at boundary of the reference capture cross section, λ_c^*, so that one start to see altered or non altered trajectories due to the stress deformation. The λ_c^* is the trajectory of the last MDCP, which would be captured by the stent wires in the rigid case.

In our mathematical model, the effective initial distance between the MDCPs at the entrance of CV is calculated from the cube root of the MDCPs amount per litre (dm^3), noting the experimental MDCP concentration as 4×10^{10} per litre [8] leads to effective initial distance of 29.24 μm.

Under the physiological loading, the behaviour of the MDCPs after agglomeration is also considered and the MDCPs create a cluster during their agglomeration. The volume of the cluster is calculated by summing the volume of the MDCPs agglomerated and the radius of the cluster is calculated using the general volume formulation ($4/3\,\pi\, r^3$) [8]. Whilst this assumption does not account fully for the resulting hydrodynamic volume, the effect of this assumption

should not significantly affect our results.

In order to describe the effect of mechanical stress deformation, in each time step we examine the effects of interactions on the CE of the system near the λ_c^* due to the changes in fluid velocity and calculated magnetic flux density. For this, we place the centre of the particle cluster on the λ_c^* for a given injection fluid velocity and record changes in CE through following the MDCP trajectories in rigid case. We then shift the particle cluster up and down, and again record changes in CE under the physiological loading. This approach is repeated for various injection fluid velocities and magnetic fields. We note that regions closest to the vessel wall do not contribute largely to the changes in CE.

Of interest is the effect of the injection velocity of the fluid and the magnetic field strength on the CE of the system in a dynamically stretched vessel (f=10 Hz). The results of this sinusoidal cyclic model are presented in parallel to the previously published rigid model [8]. Figure (2) and Figure (3) show the variation in CE of the IA-MDT system at four different applied magnetic fields strength (0.15 T, 0.30 T, 0.45 T and 0.60 T) and seven different injection fluid velocities $(0.05, 0.1, 0.2, 0.4, 1.0, 2.0, 4.5)$ with and without stretching.

In this model four different homogeneous magnetic field strengths $\mu_0 H_0 =$ 0.15 T, 0.30 T, 0.45 T and 0.60 T are applied for different flow rates (injection velocities) $0.05, 0.1, 0.2, 0.4, 1.0, 2.0, 4.5\,\mathrm{cm/s}$ as in Figures 2 and 3.

Once the magnetic field is applied under the physiological loading,the smaller number of MDCPs were seen to agglomerate and create smaller clusters comparing to the rigid case. With low fluid velocity ($\leq 10\,\mathrm{cm/s}$) and higher applied magnetic field strength ($\mu_0 H_0 =$ 0.60 T), MDCPs create a larger volume of cluster more easily than with the lower applied magnetic field strength ($\mu_0 H_0 =$ 0.15 T) and when we increase the fluid velocity the likelihood of the agglomeration of the MDCPs starts to decrease in both cases.

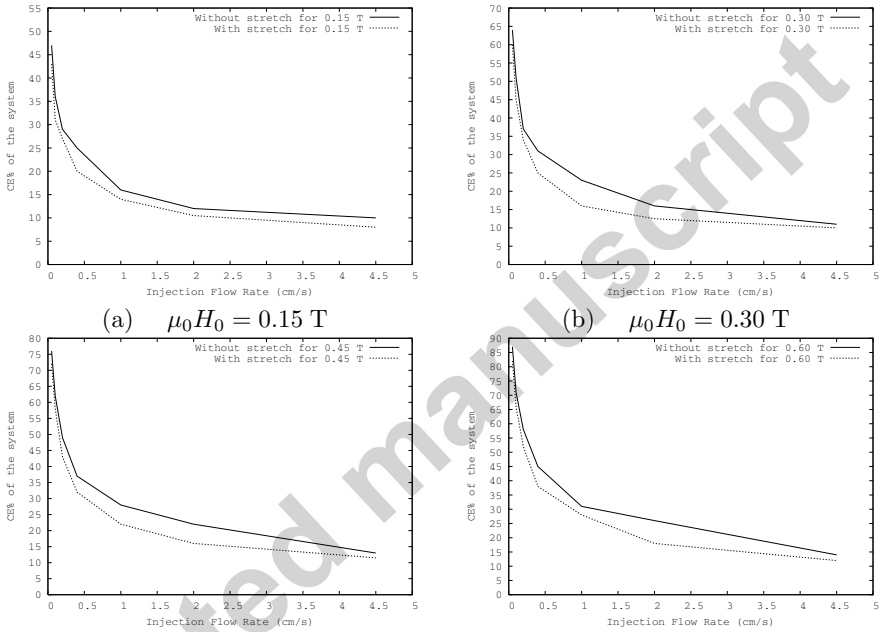

(a) $\mu_0 H_0 = 0.15$ T (b) $\mu_0 H_0 = 0.30$ T

(c) $\mu_0 H_0 = 0.45$ T (d) $\mu_0 H_0 = 0.60$ T

Figure 2: The collection efficiency (CE) of the system plotted as a function of the injection flow rate ($0.05, 0.1, 0.2, 0.4, 1.0, 2.0, 4.5$ cm/s) at the applied field a) $\mu_0 H_0$= 0.15 T, b) $\mu_0 H_0$= 0.30 T, c) $\mu_0 H_0$= 0.45 T, d) $\mu_0 H_0$= 0.60 T.

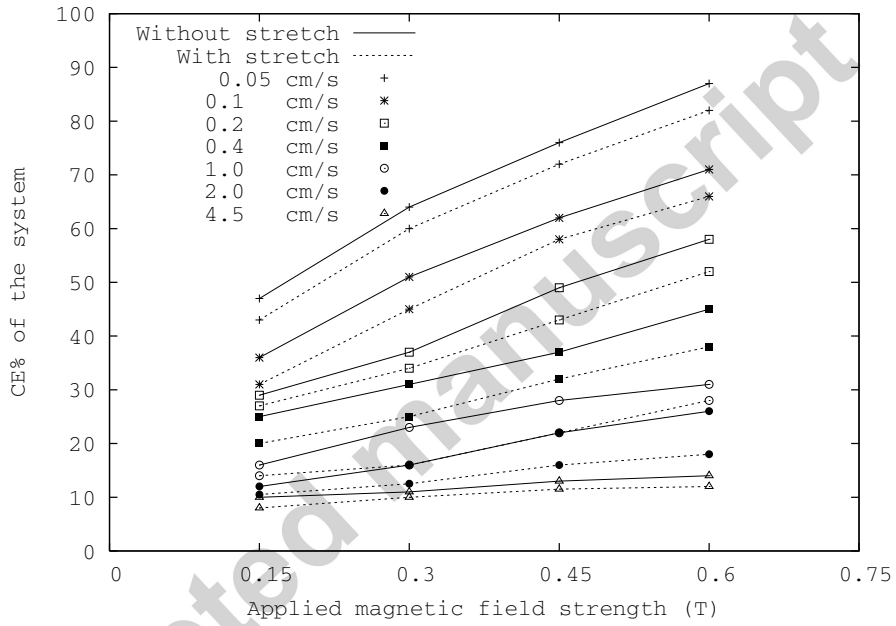

Figure 3: The collection efficiency (CE) of the system plotted as a function of the applied field ($\mu_0 H_0$= 0.15, 0.30, 0.45, 0.60 T) for different injection flow rates ($0.05, 0.1, 0.2, 0.4, 1.0, 2.0, 4.5\,\mathrm{cm/s}$).

6. Conclusions

An IA-MDT model in a mechanically stretched vessel is presented under the influence of pulsatile blood circulation. The system performance of the mathematical model can decrease by as much as 10 % due to the effects of the blood flow. This model also considered the agglomeration of particles known to occur in such systems [5, 8]. The resulting collection efficiencies derived from this new mathematical model are in agreement with previously published work [8]. In future work, we hope to present an in vitro experimental verification of this arterial vessel stretching model.

Acknowledgements

AM would like to thank Telecommunications Software & Systems Group (TSSG) for the financial support and Dr Prina-Mello would like to thank Science Foundation Ireland (SFI), and CRANN for the financial support.

References

References

[1] Q. A. Pankhurst, N. K. T. Thanh, S. K. Jones, J. Dobson, Progress in applications of magnetic nanoparticles in biomedicine, J. Phys. D: Appl. Phys. 42 (2009) 224001.

[2] A. G. Roca, R. Costo, A. F. Rebolledo, S. Veintemillas-Verdaguer, P. Tartaj, T. .Gonzalez-Carreno, M. P. Morales, C. J. Serna, Progress in the preparation of magnetic nanoparticles for applications in biomedicine, J. Phys. D: Appl. Phys. 42 (2009) 224002.

[3] C. C. Berry, Progress in functionalization of magnetic nanoparticles for applications in biomedicine, J. Phys. D: Appl. Phys. 42 (2009) 224003.

[4] A. J. Lemke, M. S. von Pilsach, A. S. Lübbe, C. Bergemann, H. Riess, R. Felix, MRI after magnetic drug targeting in patients with advanced solid malignant tumors., Eur. Radiol. 14 (2004) 1949–1955.

[5] M. O. Avilés, A. D. Ebner, J. A. Ritter, Implant assisted-magnetic drug targeting: Comparison of in vitro experiments with theory, J. Magn. Magn. Mater. 320 (2008) 2704–2713.

[6] P. J. Cregg, K. Murphy, A. Mardinoglu, Calculation of nanoparticle capture efficiency in magnetic drug targeting, J. Magn. Magn. Mater. 320 (2008) 3272–3275.

[7] P. J. Cregg, K. Murphy, A. Mardinoglu, Inclusion of magnetic dipole-dipole and hydrodynamic interactions in implant assisted magnetic drug targeting, J. Magn. Magn. Mater. 321 (2009) 3893–3898.

[8] P. J. Cregg, K. Murphy, A. Mardinoglu, A. Prina-Mello, Many particle magnetic dipole-dipole and hydrodynamic interactions in magnetizable stent assisted magnetic drug targeting, J. Magn. Magn. Mater. 322 (2010) 2087–2094.

[9] Z. S. Jackson, A. I. Gotlieb, B. L. Langille, Wall tissue remodelling regulates longitudinal tension in arteries, Journal of the American Heart Association 90 (2002) 918–925.

[10] G. A. Holzapfel, T. C. Gasser, Computational stress deformation analyses of arterial walls including high pressure response, International Journal of Cardiology 116 (2007) 78–85.

[11] P. J. Prendergast, C. Lally, S. Daly, A. J. Reid, T. C. Lee, D. Quinn, F. Dolan, Analysis of prolapse in cardiovascular stents: A constitutive equation for vascular tissue and finite element modelling, Journal of Biomechanical Engineering 125 (2003) 692–699.

[12] C. Lally, F. Dolan, P. J. Prendergast, Cardiovascular stent design and vessel stresses: A finite element analysis, Journal of Biomechanics 38 (2005) 1574–1581.

[13] M. Moretti, A. Prina-Mello, A. J. Reid, V. Barron, P. J. Prendergast, Wall tissue remodelling regulates longitudinal tension in arteries, Journal of Materials Science: Materials in Medicine 15 (2004) 1159–1164.

[14] A. Pelton, V. Schroeder, M. Mitchell, X. Y. Gong, M. Barney, S. W. Robertson, Fatigue and durability of Nitinol stents., J. Mech. Behav. Biom. Mat. 1 (2008) 153–164.

[15] M. Early, C. Lally, P. J. Prendergast, D. Kelly, Stresses in peripheral arteries following stent placement: a finite element analysis., Comput. Meth. Biomech. Biomed. Eng. 12 (2009) 25–33.

[16] OpenCFD Ltd, OpenFOAM 1.6, http://www.opencfd.co.uk (2010).

[17] T. W. Duerig, D. E. Tolomeo, M. Wholey, An overview of superelastic stent design., Min. Invas. Ther. and Allied Technol. 9 (2000) 235–246.

[18] J. Zahora, A. Bezrouk, J. Hanus, Models of stents, Comparison and Applications., Physiol. Res. 56 (2007) 115–121.

[19] P. J. Cregg, L. Bessais, Series expansions for the magnetisation of a solid superparamagnetic system of non-interacting particles with anisotropy, J. Magn. Magn. Mater. 202 (1999) 554–564.

[20] H. C. Bryant, D. A. Sergatskov, D. Lovato, N. L. Adolphi, R. S. Larson, E. R. Flynn, Magnetic needles and superparamagnetic cells, Phys. Med. Biol. 52 (2007) 4009–4025.